polymer papers

Neutron scattering studies on solution-grown crystals of polyethylene: a statistical preference for adjacent re-entry

S. J. Spells and D. M. Sadler
H. H. Wills Physics Laboratory, University of Bristol, Tyndall Avenue, Bristol BS8 1TL, UK
(Received 28 April 1983)

Neutron scattering studies of solution-grown polyethylene crystals demonstrate a strong statistical preference for adjacent re-entry, with 75% of stems occupying adjacent lattice sites. The number of sheets of stems for one molecule increases with molecular weight, with an average molecular weight per sheet of 21 000. These are the main features of computer models which give the best agreement with scattering data obtained over an angular range ($q \leqslant 1$ Å^{-1}). Scattering in this q range is directly sensitive to typical stem separations. Any preference for alternate re-entry would result in a peak at $q = 0.7$ Å^{-1}, which was not observed. The results are discussed in terms of possible crystallization mechanisms.

(Keywords: solution grown; polyethylene; neutron scattering; adjacent re-entry; conformation; crystallization mechanisms)

INTRODUCTION

Only by understanding the routes by which polymer chains enter the crystalline state can the structure of the crystals be explained. The study of crystals grown from solution led to the discovery of chain folding as a growth mechanism leading to lamellar crystallites[1]. Progress in this field has been hampered by the difficulty of defining chain conformations in the bulk state. Neutron scattering is alleviating this problem, by allowing chain scattering functions to be obtained. *In combination* with what is known independently on solution grown crystals, the scattering measured over a wide range in q ($q = 4\pi \sin\theta/\lambda$) where 2θ is the scattering angle) now leaves little ambiguity in chain conformation. This allows details of crystallization mechanisms to be related to experimental evidence.

It is known that most of the material in the crystals is contained in 'stems', the straight sequences of chains crossing the lamellae at $\approx 30°$ to the lamellar normals. This information, when used as a precondition in making conformational models, removes much of the ambiguity that is sometimes a feature of small-angle scattering. The scattering is very sensitive to the displacements of different stems from the same molecule, but much less so to the details of the folds joining the stems. Evidence for the latter is available from the body of research on the nature of the fold surface. Reviews[2-4] describe this area, and some of the conclusions are listed as follows (see especially ref. 4).

Electron microscopy demonstrates unequivocally[2,3] that the folds tend to lie preferentially in a direction parallel to the growth faces ({110} in the present case). There is however no conclusive evidence from this technique whether the folding is adjacent, or, as a special case of adjacent re-entry, whether the folds are crystallographically equivalent (or 'regular'). Evidence has accumulated that the folds occur at different heights with respect to the fold surface[5,6]. Any model of folding is also likely to predict such a result (see refs. 7 and 8). Much of the lack of complete crystallinity can be associated with the disordered fold layer of thickness ≈ 10 Å. Additional surface disorder is probably present as loops which resembles more closely a truly 'amorphous' layer. *Figure 1* summarizes these conclusions. Adjacent re-entry is shown here, and many results suggest no extensive random re-entry, but 100% adjacency is not an essential feature. The degree of adjacency is to be tested here against the neutron scattering data, and parallel experiments with infra-red spectroscopy (i.r.) lead to very similar conclusions.

Neutron scattering has demonstrated a marked difference in conformation between melt-grown and solution-grown crystals[9-11]. The scattering curves are completely different and intensities can differ by an order of magnitude (see *Figure 10*).

Published neutron scattering results on solution-grown crystals have all been interpreted[9-14] in terms of sheet-shaped entities within the whole molecule, as was anticipated (see *Figure 2* which shows the conformation in a perspective diagram). However, the conformation was not the idealized one of a single molecule forming one uninterrupted adjacently folded ribbon, and this also was not unexpected especially as the neutron scattering experiments were necessarily carried out on crystals grown at high supercoolings. On the basis of the scattering, two structural features seemed unavoidable; (a) superfolding and (b) stem dilution.

(a) Radii of gyration were found to be insensitive to molecular weight, suggestive of ribbons folding back on themselves[11]. In addition intensities decreased with angle faster than would be expected for single sheets[9,10], and this could be explained by interference between successive sheets in the superfolded structure.

(b) The calibrated scattering intensity was too low for

0032-3861/84/060739-10$03.00

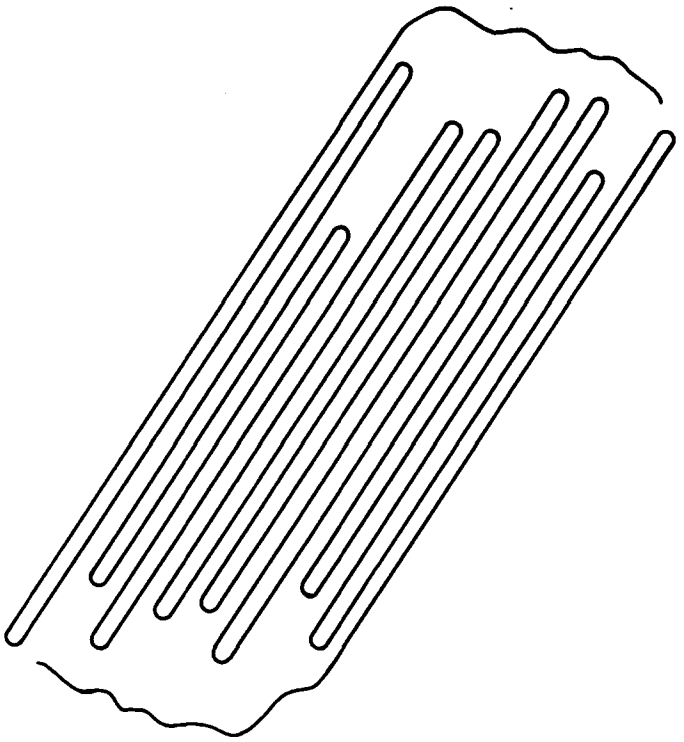

Figure 1 Schematic diagram showing the probable nature of surface disorder in solution-grown crystals of polyethylene[2-6]. Disorder occurs as a result of fluctuations in fold positions and also because of superficial loops. The exact degree of adjacency of folding is arbitrary (*cf.* later Figures)

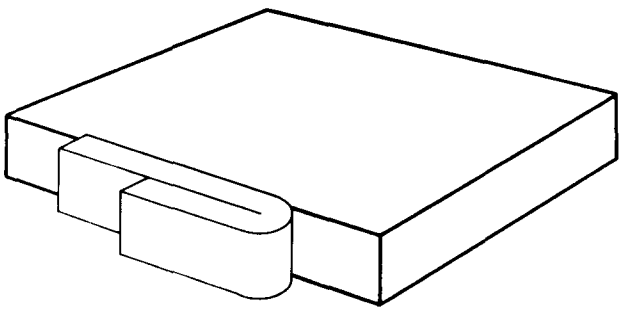

Figure 2 Sheet-like conformation as a result of folding (schematic, see text)

the folding all to be adjacent, by a factor of approximately two[10,13]. In the original work from the Bristol laboratory[9,10] (a) and (b) were apparent from the two parameters D (apparent thickness of sheets) and n_A (scattering density of sheets). n_A was always approximately a factor of two too low for pure adjacent re-entry, given the number of sheets derived from D. A subsequent analysis by Yoon and Flory[13] centred on the dilution, and explained it by a preference for 'alternate' folding, i.e. a stem separation of 8.8 Å. (In addition, infra-red spectroscopy showed that the folding was not consistently adjacent[15,16].) Clearly, measurements at angles approaching the crystallographic region are necessary to investigate this possibility. Wide-angle neutron scattering (WANS) measurements have been reported recently for isotopic blends of PE[17,18]. No peak was reported in the region corresponding to a separation of 8.8 Å, although in both cases the aim was to search for diffuse peaks arising from adjacent folding in the (100) and (010) planes. By contrast, the measurements presented here are discussed in terms of the grouping of chain stems within superfolded sheets.

It is not yet possible to specify in detail a model for crystallization which would predict dilution and superfolding. One class of models is based on Regime I type crystallization, i.e. only one re-entrant corner exists on each growth face[19,20]. If a molecule attaches at its centre, one part will crystallize as one ribbon, and the second part is free to crystallize in a second ribbon. However, if many niches are present, for kinetic[21] or other[22] reasons, a molecule should attach independently at different points along its length.

EXPERIMENTAL

Sample preparation and characterization

Mixed-crystal mats of PE were prepared from xylene solution as previously described[10] using a crystallization temperature of 70°C. PE samples crystallized at higher polymer concentrations were prepared by mixing mixed-crystal material with liquid paraffin, and maintaining a temperature just above the polymer melting temperature for several hours under vacuum before quenching into water. The samples were washed with xylene and pressed. They were then washed with acetone before drying. Mixed crystals of dotriacontane ($C_{32}H_{66}$) were prepared by the evaporation of solvent from solutions of the paraffins in benzene, followed by pressing directly into sample holders. Paraffin crystals of this type have been used previously as model systems with a random arrangement of molecular stems, because chain folding is absent[12,15]. They serve the same purpose here.

PE starting materials were prepared by liquid–liquid fractionation and the molecular weights were determined by g.p.c. Samples were prepared for various 'guest' concentrations, using either PED or PEH as the matrix. It has been reported that for identical crystallization conditions, the long spacings for isotopic mixtures vary considerably with isotope proportions[12]. Measurements of X-ray long spacings and Raman (LA mode) long spacings for crystals grown from xylene solution have shown that there is little variation with PEH concentration for between 5 and 20% PEH. In these cases, long spacings were between 100 and 105 Å, whereas for PEH matrix samples, figures of 110 to 115 Å were obtained. Sample crystallinity, from d.c.s. measurements, was $\approx 65\%$.

Crystal orientation in the sedimented mats was monitored using both wide- and small-angle X-ray diffraction. In the former case, the azimuthal intensity distribution of the (110) peak includes contributions from planes parallel to the crystal growth faces and also from equivalent planes which are not growth faces. The crystal misorientation necessary for planes to be in a diffracting condition is different in the two cases. However, at small angles, the long spacing shows an azimuthal intensity variation which corresponds to the distribution in crystallite orientation. This was used to determine the expected enhancement in neutron scattering intensity, as described later.

PE samples crystallized from liquid paraffin mixtures showed long spacings of between 120 and 170 Å, the spacing increasing with polymer concentration in paraffin.

The restriction of previous SANS measurements to PE crystallized at high supercoolings had been mentioned previously. This is to minimize isotopic fractionation. The additional signal arising from fractionation is, however,

restricted to small angles, decaying approximately as q^{-4} [10]. WANS measurements are, therefore, insensitive to such effects.

Neutron scattering experiments

The angular ranges of scattering experiments can conveniently be classified, together with instruments principally used, as follows:

(1) Small-angle (SANS) $q<0.1$ Å^{-1}. The D17 multidetector instrument (ILL) was used here (the sister instrument D11 is described in ref. 23).

(2) Intermediate angle (IANS) $0.4>q>0.1$ Å^{-1} D17 was used.

(3) Wide-angle (WANS) $q>0.4$ Å^{-1}. The single detector Guide Tube diffractometer (Harwell) was used in this region[24].

The neutron wavelengths used for individual measurements are shown with the scattering data. The D1B curved multidetector system (ILL) was also used.

Analysis of neutron scattering data

Background subtraction. In the WANS range, the PEH concentration used for samples is a compromise between 2 factors: the diffuse scattered intensity is intrinsically small and the incoherent signal from PEH is large. Therefore, PEH concentrations of typically 10% were used. At this concentration, and with the small net signal, it is important to use the correct combination of PEH and PED background runs for subtraction from the raw sample data.

If the average scattering length for hydrogen isotopes is $\bar{b}$, then for isotope i the scattering length may be written as $\bar{b}+\delta b_i$. The scattering amplitude from a sample may then be written as:

$$A(\underline{q})=\sum_i\sum_j(\bar{b}+\delta b_i)A_iA_j+\sum_i\sum_j b_i'A_iA_j \qquad (1)$$

where A_i and A_j are the scattering amplitudes corresponding to the centres of gravity of molecules i and the displacements of atoms j within the molecule. The b_i' are the scattering lengths of atoms other than hydrogen. Collecting terms in $\bar{b}$ and b_i', and setting cross terms equal to zero on the assumption of random isotopic mixing:

$$|A(\underline{q})|^2=|A_0(\underline{q},b)|^2+\sum_k\delta b_k^2(n^2(P_k(\underline{q}))N_k \qquad (2)$$

with n the number of hydrogen atoms per molecule, $P_k(q)$ the scattering function for a single molecule and N_k the number of molecules of isotope k.

The final term in equation (2) contains the information primarily required from neutron scattering experiments, but the first term on the right-hand side must first be subtracted from the total intensity, $|A(\underline{q})|^2$. For small-angle scattering, the PED concentration is usually very small, so that $\bar{b}\approx b_H$. However, with typically 10% of PEH in the samples used here, it was necessary to use the appropriate value of $\bar{b}$.

Calibration. Incoherent scattering from pure PEH and from water was used to calibrate the intensity, and also the method described by Jacrot[25,26]. Similar results were obtained in all cases.

Methods of calculating the scattered intensity. Equation (2) may be rewritten in terms of the macroscopic scattering cross section, $d\Sigma/d\Omega$:

$$V\frac{d\Sigma}{d\Omega}=|A(\underline{q})|^2$$
$$=|A_0(\underline{q},\bar{b})|^2+N(nP(q))c_Dc_H(b_D-b_H)^2 \qquad (3)$$

where V is the sample volume, $|A_0(\underline{q},b)|^2$ is the density fluctuation term, N the number of hydrogen atoms and c_D and c_H the volume fractions of PED and PEH in the sample[4]. As in previous work[10] the normalized intensity $I(q)$ is $nP(q)$. In equation (3), $P(q)$ derives mainly from the minority component in the isotope mixture.

The scattered intensity for any arrangement of monomers may firstly be represented in terms of the separations r_{ij} between ith and jth hydrogen atoms by the Debye relation for isotropic samples:

$$P(q)=\sum_i\sum_j\frac{\sin(qr_{ij})}{qr_{ij}} \qquad (4)$$

Several approximations may now be made. From the description given of the nature of the disorder in these crystals, the proportion of the monomers which are either in stems, or displaced only slightly from the line of the stems, is probably higher than given by a simple measure of crystallinity. Equation (4) was not used in general because the computation times would be far too long for a reasonable number of models to be tested. Furthermore, a large amount of conformational detail (which is not important in determining the intensities) would have to be specificed and orientation effects complicate an equation such as equation (4). Instead, the calculation is made over stems only.

Infinitely thin, long stems scatter according to:[27]

$$I_c(q)=n_L\frac{\pi}{q} \qquad (5)$$

A parallel pair of such stems separated by a distance R gives:[28,29]

$$I_c(q)=\frac{1}{2}\left(n_L\frac{\pi}{q}\right)(1+J_0(qR))$$

This can be generalized to:

$$I_c(q)=\frac{1}{N}\left(n_L\frac{\pi}{q}\right)\sum_i^N\sum_j^N J_0(qR_{ij}) \qquad (6)$$

where N is the number of stems, or, alternatively:

$$I_c(q)=\left(n_L\frac{\pi}{q}\right)\int\Gamma(R)J_0(qR)dR \qquad (7)$$

where $\Gamma(R)$ is a correlation function for the stems.

Account must now be taken of the atomic structure of the stem. The ratio of the scattering from one stem, calculated from equation (4)m to the scattering from a thin stem (equation (5)) is defined as $C(q)$. An approximation is made that the intensities in equations (6) and (7) may be corrected for the atomic structure by multiplying them by the same factor $C(q)$. Accordingly, the experimental intensities are used to calculate the equivalent

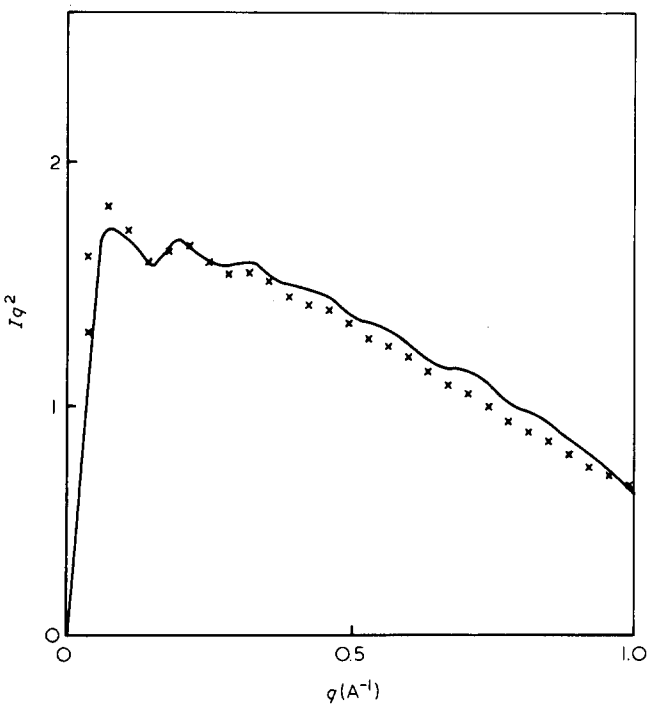

Figure 3 Calculated 'Kratky plots' of $I(q)q^2$ versus q for a sheet of 10 crystal stems. The solid line is derived from the Debye equation, equation (4) and the crosses from the assumption of long, thin stems (Equation (6)). For another comparison between the two methods of calculations see Figure *A* of ref. 29

intensities for infinitely thin stems, $I_c(q)$, defined as $I(q)/C(q)$. The standard form for plotting intensities in this work is as $I_c(q)q^2$ *versus* q. In this format, a system of isolated stems would yield a straight line plot through the origin. This provides a convenient way of illustrating departures from isolated stem scattering: any grouping of stems (for example, in sheets) will produce a modification of the interference between stems.

Figure 3 shows intensities $I(q)q^2$ calculated using equations (4) and (6) for similar structures of 10 stems in a row forming a sheet. In the case of equation (4) the stems have a finite length of 100 Å. The ripples are due to the finite dimensions of the sheet. In practice $C(q)$ can be calculated over a wide range of q by the exponential approximation[10], with the root mean square radius of the hydrogen atoms from the stem as 1.46 Å.

The methods of calculation based on equation (6) apply only when q is $>1/l$ where l is the stem length (at $q>0.1$ Å^{-1} in *Figure 3*, and also for the actual crystals).

Orientation corrections. Most experiments were carried out on mats, during the preparation of which the lamellar normals $\underline{n}$ and $\langle 001 \rangle$ direction become preferentially oriented along the normals to the mats $\underline{m}$. There is then an axis of fibre symmetry along $\underline{m}$. The degree of orientation is reproducible from one mat to another. The scattering from the stems is only significant when the vector $\underline{q}$ is perpendicular to the chain axis (the c-direction). Hence, with the usual experimental situation of $\underline{m}$ along the beam direction, the intensity is enhanced above what it would be for isotropic samples. The enhancement factor E is likely to be independent of q at sufficiently large q, and this is confirmed by the comparison in *Figure 4* between oriented and isotropic samples. Clearly, E will decrease to a limiting value of unity as q goes to zero (the 'forward scattering' for the whole molecules $I(0)$, is independent of azimuthal angle).

E was evaluated in three ways. Firstly the ratio of the two intensities in *Figure 4* gives a value approaching 2.0 at widest angles. Secondly, rocking curves were obtained on the Guide Tube Diffractometer, giving a value of ≈ 1.8. Thirdly, orientation functions were obtained for $\underline{n}$ (by small-angle X-ray scattering) and for {110} crystal planes by wide-angle X-ray diffraction. To a first approximation, E for sheets of stems along {110} can be taken directly from the 110 X-ray peaks, by integrating over the experimental distribution of peak intensity and comparison with an integral assuming isotropy. On this basis E is 2.1. The sedimentation of the lamellar crystals involves the collapse of structures which are tent-like in suspension[30]. This means that {110} planes which are along the growth faces of the lamellae (i.e. along the rims of the tents) will be slightly more misoriented that the other {110} planes. The value of E obtained on this basis is not greatly different, as explained in the following.

The degree of orientation for the two sets of {110} planes can be distinguished by a detailed analysis of the orientation functions, making use of the properties of Legendre polynomials. p is defined as the first-order coefficients of the orientation distribution, given by:

$$\frac{1}{2}\left\{\frac{3\int n_\gamma \sin\gamma\cos^2\gamma\,d\gamma}{\int n_\gamma \sin\gamma\,d\gamma} - 1\right\}$$

where n_γ is the number of vectors making an angle γ with an axis (e.g. n). In the case of normals to diffracting planes, n_γ is taken to be proportional to the corresponding diffraction intensity, and is measured using densitometer traces of X-ray diffraction patterns. p_1 (for normals to diffracting planes) can be calculated from p_2 (for the orientation of $\underline{n}$ with respect to $\underline{m}$) and p_3 (for the orientation of the lattice plane normal with respect to $\underline{n}$): $p_1 = p_2 p_3$. The value of p_3 is known from electron microscopy, based on the lamellar surfaces being approximately parallel to {314} planes[30]. Self consistency can be tested by calculating p_1 for all {110} and

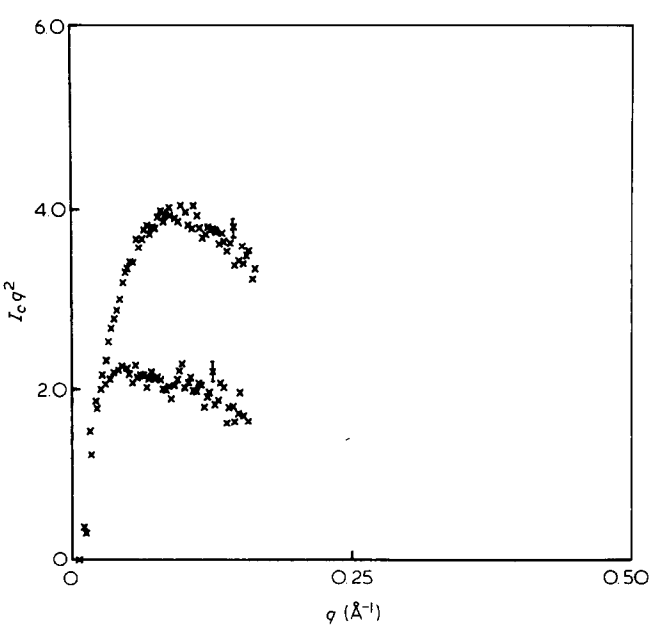

Figure 4 SANS results for a sample with 3% PED ($\bar{M}_w = 103\,000$); crystallization temperature 70°C. The upper curve is from an oriented mat and the lower curve from an isotropic sample. Neutron wavelength 6.0 Å

comparison with X-ray diffraction measurements of (110) peaks: -0.266 and -0.261, respectively. p_1 for growth planes {110} can now be calculated separately, at -0.242. (Note: 'perfect' fibre orientation corresponds to $p_1 = -0.5$).

The orientation distribution for all {110} planes is given by wide-angle X-ray diffraction: the width of this distribution was increased (keeping the shape constant) so as to give a p_1 value of -0.242. From this curve E was calculated for growth faces (in the same way as for the average {110} orientation) to be 1.74.

Effects of amorphous content. The crystals have crystallinities of ≈ 0.65. The non-crystalline component will consist partly of loops on the surface which are best described as truly amorphous. However, the proportion of this material will be less than 0.35 as some of the disorder will occur as a result of poor packing of stems in the fold region (*Figure 1*). The effects of the latter can be allowed for in the hypothesis that the material in the fold regions is in the form of extensions to the stems to which they are attached (*Figure 1*). The effects of the approximation have been shown previously to be small for relatively large distances between stems (40–69 Å, which is much larger than for the preferred model). Any discrepancy between the true scattering and that from a system with crystal stems extended to allow for material from the fold regions, therefore, is even smaller for the model discussed here.

For long loops on the surface one may expect a scattering similar to that of amorphous polyethylene, which for much of the q range involved is small compared with that from the crystal. However, for $q \simeq 1.3$ Å^{-1} the scattering from single stems with no defects is very small, so an amorphous contribution may then be apparent. This is a higher value of q than used to compare predictions with experiment. It is simply noted here that the intensity immediately before the (110) peak was found to increase more rapidly than predicted for the preferred model. In the region of $q = 1.3$ Å^{-1}, the experimental scattering was $\simeq 1.7$ times larger than predicted. An extension of previous intensity calculations[29] to this range of q shows this to be consistent with a proportion of 0.35 of material being in the form of long loops. In view of the marked simplifications involved in these estimates, the agreement between 0.35 and the nominal amorphous content is probably fortuitous.

In practice it is not possible to quantify the two sources of disorder, surface loops and fold disorder, so for presentational purposes the experimental intensities are divided by the crystallinity fraction. Hence, the experimental intensities which are shown are upper limits to the true values.

The integrated intensities. General arguments can show that the integral of $I_c(q)q^2$ over a q range up to the first diffraction maximum is insensitive to the details of the conformation. Consider as an analogy the one-dimensional structure of a series of points all separated by the same distance d. Then the integrals with each of the terms in equation (4) with $i \neq j$ (the 'interference' terms) have the property:

$$\int_0^{2\pi/d} q \frac{\sin(qr_{ij})}{qr_{ij}} dq = 0$$

As all separations $r_{ij} = nd$(n integer), $I(q)q$ has the property that its integral from $q = 0$ to $q = 2\pi/d$ does not depend on the interference terms. Similarly, if most R_{ij} in equation (6) are multiples of the nearest neighbour distance, the integral of $I_c(q)q^2$ over the equivalent limits is only sensitive to the $i = j$ terms (the 'single stem' scattering) and much less so to the $i \neq j$ terms (i.e. those that are conformation dependent). This is only an approximate dimensional argument, for obvious reasons, but it has been verified to within $\approx 5\%$ by the expedient of calculating $I_c(q)q^2$ numerically for widely differing models. If $I_c(q)$ is greatly in excess of the single stem scattering at small q (e.g. solution-grown crystals) there must also be a compensating decrease below the single stem scattering at large q. This argument is also relevant to the scaling procedures discussed previously. Uncertainties in the scaling factors will result in discrepancies in the integrated intensity function (which is model insensitive) but not in the q dependence of the intensities (which is model sensitive).

RESULTS

Neutron scattering

WANS results for a 10% blend of dotriacontane in d_{66}-dotriacontane are shown in *Figure 5*, together with the scattering expected for stems only. The deuterated paraffin background data has been scaled by the same factor as for PE samples. The sample scattering clearly shows close agreement with the line indicating that molecules are arranged randomly within the crystals. Any modification in the WANS intensity in the case of PE mixed crystals can therefore be attributed to a more ordered array of chain stems.

SANS/IANS data for PE mixed crystals for a range of 'guest' molecular weights are shown in *Figure 6*. Other than for very low molecular weights, the curves all show maxima within the range of q from 0.05 to 0.15 Å^{-1}, the

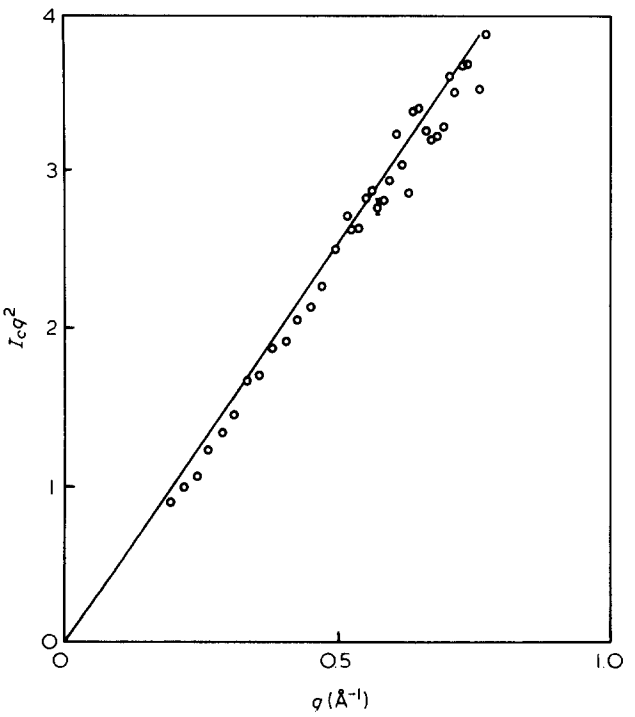

Figure 5 Scattering data for 10% dotriacontane in d_{66}–dotriacontane (isotropic). Wavelength = 4.76 Å

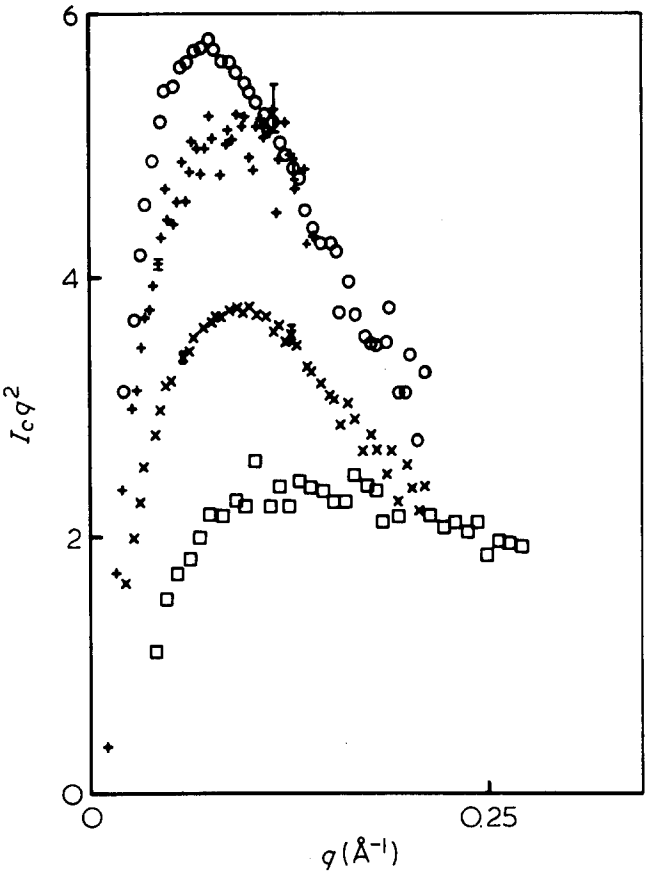

Figure 6 SANS data for samples crystallized at 70°C. ○, 3% PED (M_w=386 000; λ=10.2 Å); +, 3% PED (M_w=189 000; λ=6.0 Å); ×, 3% PED (M_w103 000; λ=8.2 Å); □, 10% PEH (M_w=29 000; λ=8.2 Å)

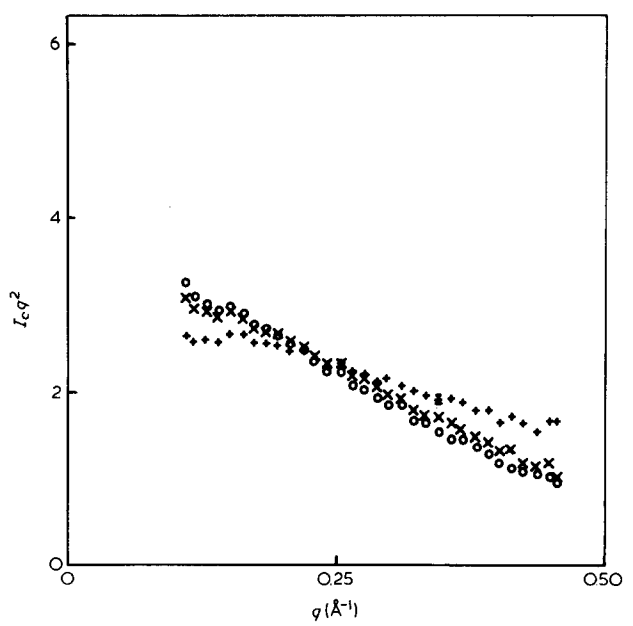

Figure 7 IANS data for samples crystallized at 70°C. ○, 5% PEH (M_w=51 000); ×, 5% PEH (M_w=29 000); +, 5% PEH (M_w=15 000); neutron wavelength=7.8 Å

position of the maximum decreasing in q as the molecular weight increases. The negative slopes of the scattering curves at larger scattering vectors show an increasing trend with increasing molecular weight.

The variation of scattered intensity with molecular weight becomes less marked as the WANS region is approached (*Figure 7*). The scattering curves cross one another within the region $0.2<q<0.3$ Å^{-1}. Within the WANS region (*Figures 8* and *9*) there is no systematic variation in sample scattering beyond $q\approx0.4$ Å^{-1} for molecular weights of between 15 000 and 87 000 ($\bar{M}_w$). It is noteworthy, however, that the scattered intensity from PE mixed crystals attains a minimum value which is smaller than that from paraffin mixtures for similar q values (*Figure 5*) by a factor of 2–3. The angular dependence is also clearly different.

The influence of crystallization conditions is demonstrated for the small-angle region in *Figure 10*. For PE crystals grown from dilute xylene solution, the SANS intensity is much larger than for material quenched from the melt. The latter sample type has been shown to give IANS curves consistent with a 'subunit' model of short rows of stems connected by longer folds[29,31]. The sample crystallized from a 20% mixture with liquid paraffin clearly produces a similar scattering curve to that of the quenched material. The influence of polymer concentration in the crystallization solvent is currently

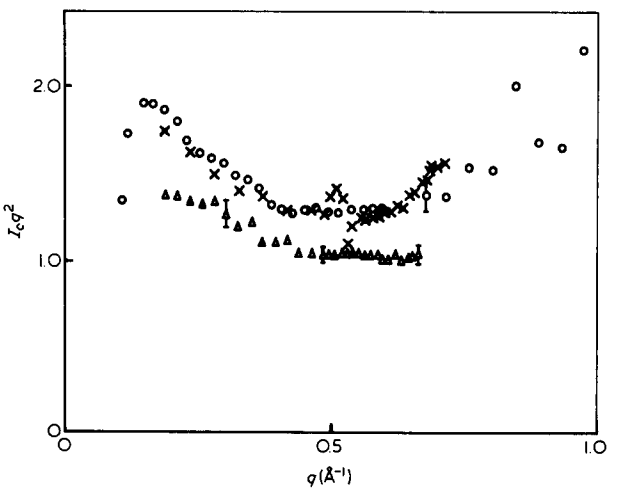

Figure 8 WANS data for samples crystallized at 70°C. ×, 10% PEH (M_w=51 000; λ=4.7 Å); ○, 10% PEH (M_w=29 000; ×λ=2.5 Å); △, 10% PEH (M_w=15 000; λ=4.7 Å)

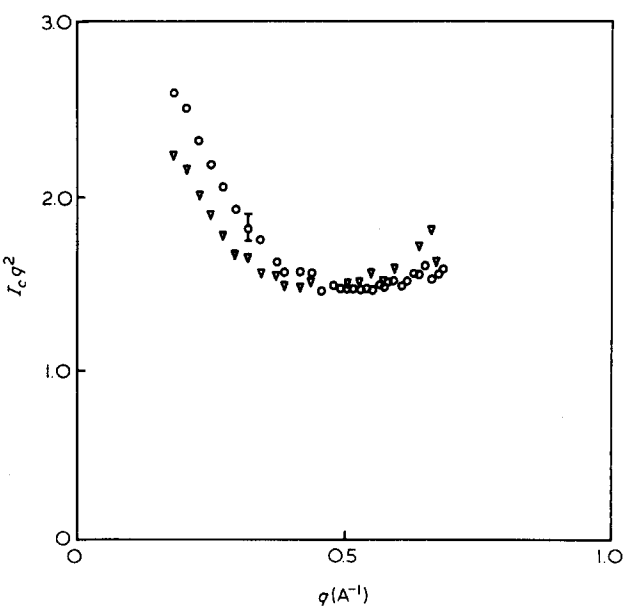

Figure 9 WANS data for samples crystallized at 70°C with λ=4.7 Å. △, 10% PEH (M_w=87 000); ○, 10% PEH (M_w=70 000)

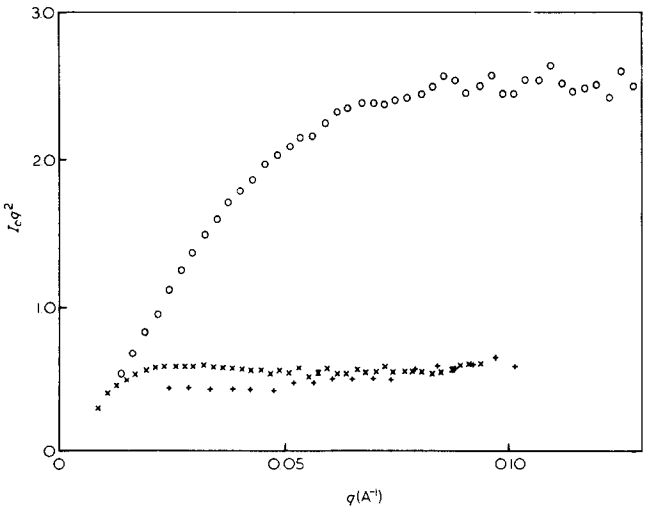

Figure 10 Variation in scattered intensity with sample type. ○, 1% PED (M_w=64 000) crystallized from dilute xylene solution at 70°C (λ=9.9 Å); ×, 3% PED ($\bar{M}_w$=59 000) crystallized from a 20% mixture with liquid paraffin (λ=10.50 Å); +, 3% PED ($\bar{M}_w$=54 000) quenched from the melt (λ=5.0 Å)

being examined in more detail: it is sufficient here to note that these results are consistent with the conformation becoming more randomized as the concentration of polymer is increased.

Computer models

Consider the stem arrangements in a sheet, given an overall dilution of a single molecule by 50%. In terms of realistic crystallization mechanisms, it is possible to envisage models which are very elaborate in terms of the number of parameters involved; the emphasis here is to minimize the elaboration rather than to produce a model which fits closely a very specific crystallization mechanism. To produce a dilution two simple models immediately appear to be appropriate: random dilution and alternate folding. However, neither is adequate, which is explained as follows.

A significant simplification in the type of folding statistics which need be considered is provided by the following. The neutron scattering technique relies on the assumption that the two isotopic species in the mixed crystals behave identically, apart from the different neutron scattering lengths for hydrogen and deuterium. With this assumption, polymer molecules must show the same crystallization behaviour, irrespective of isotope label. In particular, both 'guest' and 'host' molecules must have the same probability of depositing a second stem adjacent to a stem of the same molecule. This requirement restricts the possible overall dilution along the fold plane to ratios of integral numbers of stems (i.e. 1/2, 1/3, 1/4 etc.). A dilution of 50% satisfies this requirement for 'dilution by integers', and is within the range previously determined fron SANS and infra-red data[15].

A detailed model of crystallization should predict the details of the way the stems from two molecules (each one '50% diluted') are intermixed. For example, a Regime I mode of nucleation could involve the 'competition' between two molecules for the niche site. Two assumptions are now made. First, if molecule 1 has just contributed a stem to the crystal, the probability of the next stem being from molecule 1 is likely to be enhanced. Secondly, it is assumed that the occupation probability, p, depends only on the type of chain occupying the preceding site. For example, a value of 0.75 for p satisfies the first assumption and gives a probability of site occupancy of 0.75 if the preceding site is occupied by the labelled chain. If only two chains are crystallizing together and the unlabelled chain occupies a site, then the probability of the labelled chain occupying the next site is simply $(1-p)$.

The extent to which the stems are grouped in rows with adjacent re-entry then depends on the value of p. Consider the extreme cases: firstly, when p is very small, there is a preference for gaps between stems. With an overall dilution of 50%, this implies a regular alternation of molecular labels along the fold plane. Regular alternate re-entry would create an additional periodicity of 8.8 Å, with a peak at $q=0.7$ Å^{-1}. Conversely, if p is very large, there is a preference for the stems to be grouped together in long rows with adjacent re-entry and with long gaps between rows of stems belonging to the same molecule. Midway between the two extreme cases lies the model of random dilution, where the deposition of one stem is equally likely to be followed by a stem from either the same or a different molecule.

It is possible that the arrangement of stems in one sheet influences the arrangement of stems in the next sheet deposited in a superfolded conformation. Hence, the probability of a stem depositing at a particular site may be correlated with the presence of a stem at a neighbouring site on the previous fold plane. It is shown later that the effect of any such correlation of stem positions between sheets is less significant than the correlations of stem positions within a sheet.

Superfolding means that on some occasions a non-adjacent fold involves a complete departure from a sheet, followed by incorporation in a separate sheet. No attempt is made to specify the origin of this effect, rather the number of stems in a sheet is allowed to vary randomly, typically between 10 and 20.

A number of 'molecules' were generated with a computer, with the use of random number generation. The average correlation function $\Gamma(R)$ was then calculated and, hence, $I_c(q)$. *Figures 11* and *14* both include $I_c(q)q^2$ curves for 0.25 and 0.75 values of p. In both cases these tend to converge at the smallest values of q, but at $q>0.3$ Å^{-1} there is a marked difference according to the p value. A small p value (preference for alternate folding[13]) can be excluded because the predicted peak is not observed. The limited q range in *Figure 14* prevents any definite conclusion for the sample with $\bar{M}_w$=87 000, but the scattered intensity agrees more closely with the model of preferred adjacent re-entry over the experimental range. The effect of adjusting the degree of correlation between stem sites in neighbouring sheets is shown in *Figure 12*. Differences in the form of the scattering curves are clearly small compared with those in *Figures 11* and *14*, and as a first approximation the degree of correlation has been maintained constant and equal to zero in the models shown later.

To limit the variables used to fit data for samples of different molecular weights, the probability p was maintained constant in all the following models (see above) and the average number of sheets was allowed to vary.

In the real situation of a polymer crystallizing, some variation in the number of stems in a single sheet is clearly possible. Such a variation was incorporated in the model.

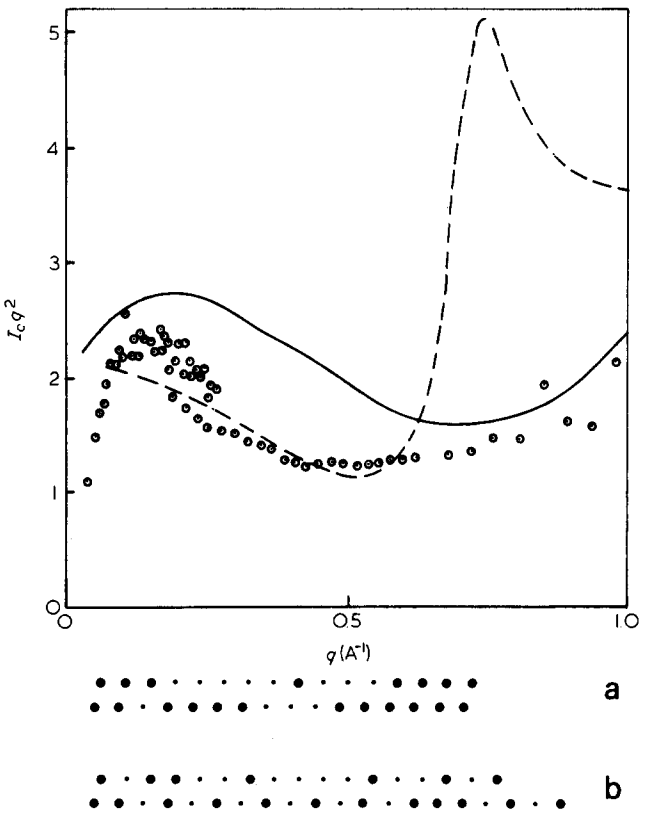

Figure 11 Composite scattering curve for a sample crystallized at 70°C. (○) with 10% PEH (M_w=29 000) (SANS (λ=8.2 Å, IANS λ=2.5 Å). The solid curve shows calculations for 75% adjacent re-entry (model (a)) and the broken curve a preference for alternate re-entry (25% adjacent, model (b))

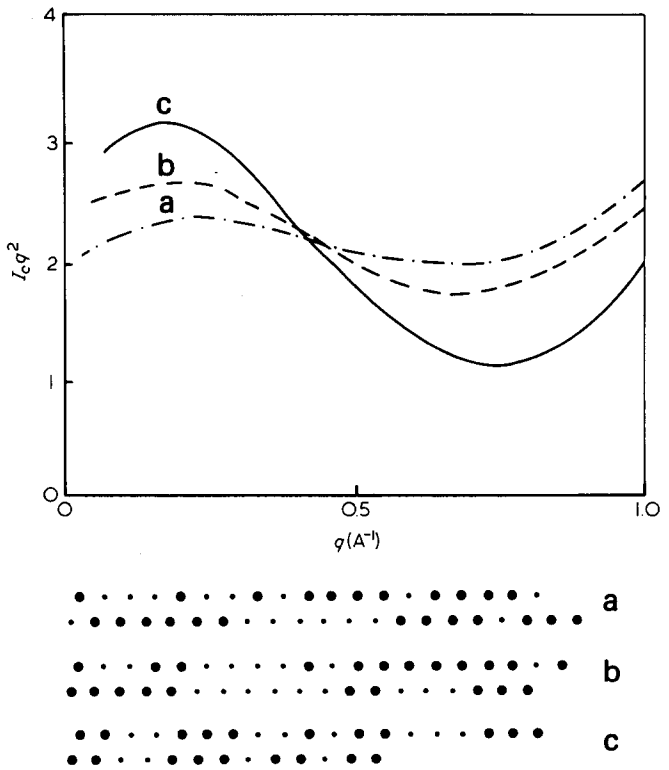

Figure 12 The effect of correlation between stem positions in adjacent sheets for 2 sheet computer models. The degree of correlation between stem positions increases from (a) to (b) to (c)

In reality, the number of sheets occupied by an individual molecule may also vary. Taken together with the polydispersity of labelled molecules, the implication is that the average value of the number of sheets used in a model to fit experimental data need not be an integer.

Figure 13 shows scattering curves for models with adjacent re-entry and between 1 and 6 sheets. The numbers of sheets giving the best fit for individual samples used are listed in *Table 1*. As examples, *Figures 11* and *14* show data for samples of $\bar{M}_w$=29 000 and 87 000, compared with the 2 and 4 sheet model calculation. The

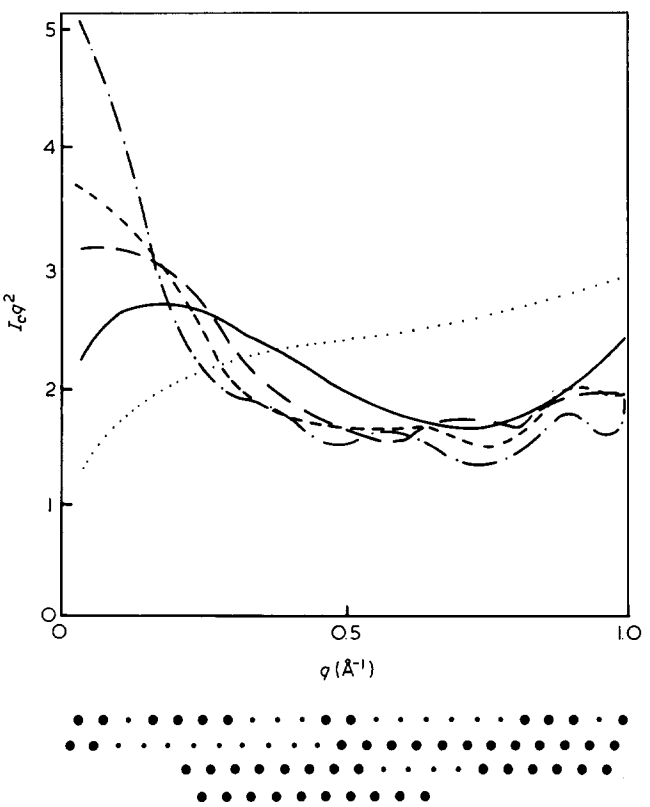

Figure 13 Computed scattering curves for a model with 75% adjacent re-entry of stems. The curves correspond to models with different numbers of sheets:–···, 1;——, 2;– –, 3;– – –, 4;–·–, 6. The stem projection shows a typical arrangement for a 4 sheet structure; the probability of adjacent re-entry p is 0.75 for all cases

Table 1 Parameters of models used in fitting experimental scattering curves

Sample	Matrix[a]	Average number[b] of sheets (n)	$\bar{M}_w \times 10^{-3}$	$\bar{M}_w \times 10^{-3}/n$
1[c]	H		386	
2	H	7	216	31
3	H	5	118	24
4	D	4	87	22
5	D	4	70	17.5
6	D	2	51	35.5
7	D	2	29	14.5
8	D	1.25	15	12
			Average	21

[a] H = PEH matrix; D = PED matrix
[b] As measured by g.p.c.
[c] For this sample, the molecular weight is too high to fit the experimental data to model curves and obtain n to sufficient accuracy

results clearly favour a preference for 75% adjacent re-entry.

It is noteworthy that the ratio $\bar{M}_w/n$, shown in *Table 1*, changes only by a factor of ≈ 2.5 for a 14 fold variation in $\bar{M}_w$. This indicates that the average length of a sheet of stems along the fold plane does not change much as the molecular length increases. Hence, the probability of a molecule folding back on itself is relatively insensitive to molecular weight confirming a result implicit in earlier SANS work[11].

These results may be compared with earlier measurements of the radius of gyration of similar samples[11]. Taking a representative long spacing of 102 Å

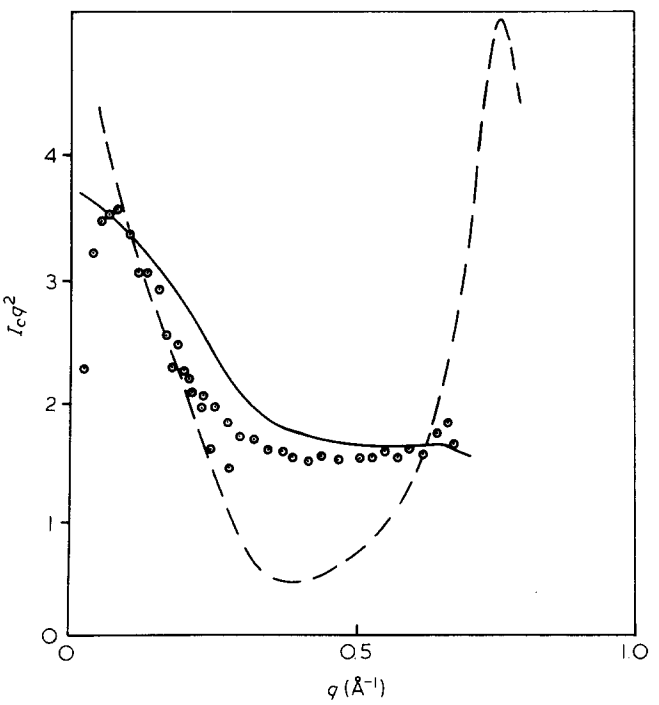

Figure 14 Composite scattering curve for a sample crystallized at 70°C (○) with 10% PEH ($\bar{M}_w$=87 000) (SANS λ=4.7 Å, IANS λ=8.2 Å). The curves show calculations from models with the same stem site statistics as in Figure 11, but both involve 4 sheets

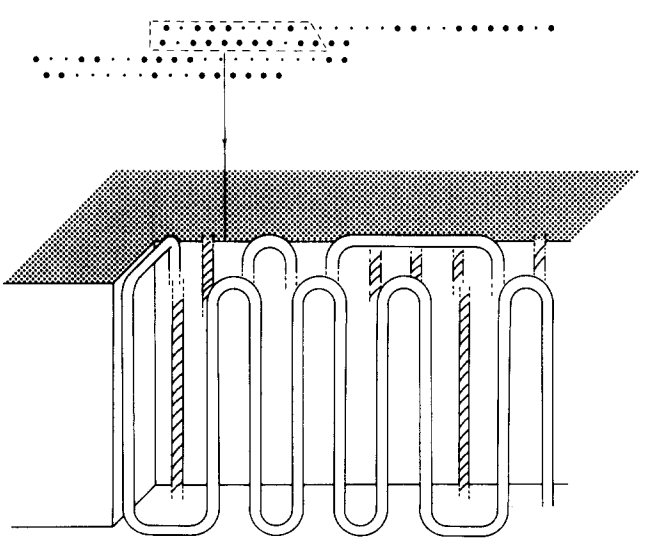

Figure 15 Perpsective diagram of the arrangement of the part of one molecule (unmarked 'chain') and its neighbours (shaded) within the crystal lattice, for the model with 75% adjacent re-entry. The corresponding stem arrangement is shown above, in projection, with large spots corresponding to the unmarked chain in the perspective view

Table 2 Distribution of stem separations for models shown in *Figure 15*

Separation between consecutive stems (Number of lattice sites)	Probability (%)
1	75
2	7
3	5
4	3
>4	9

and a tilt of 30°, the molecular weight per stem is 1330. Consider a stem arrangement with 4 sheets. Using the average value of 21 000 for $\bar{M}_w/n$ (*Table 1*), the radius of gyration can be calculated, with the assumption that the 4 sheets are in register. This gives a figure of 55 Å for the in-plane dimension (R_x), which is smaller than a value of $\approx$70 Å, interpolated from experimental data in refs. 11 and 37. The discrepancy may be largely a result of the lack of register of rhe ends of successive sheets, a feature which is incorporated in the computer models here (e.g. stem projection in *Figure 15*): this may extend the length of the molecular conformation along the fold direction to as much as twice the length of an individual sheet.

An example of the preferred models is shown in perspective and projection in *Figure 15*. It is noteworthy that the analysis of neutron scattering data only gives information on the arrangement of crystal stems, without detail of the fold conformations. The arrangements of fold drawn in *Figure 15* is the simplest case, with short folds linking the stems in each sheet: it seems reasonable to assume that the molecule should follow the growth face. *Table 2* lists the probabilities of different fold trajectories for the models corresponding to *Figures 13* and *15*. This shows the strong preference for adjacent re-entry, with 75% of folds connecting stems at adjacent sites. Infra-red measurements on similar PE mixed crystal samples have shown that the CD_2 bending vibration for the range of 'guest' molecular weight studied here invariably has a complex multiplet structure[32,33] with the splittings of the component doublets corresponding to smaller numbers of stems than in the complete molecule. This confirms that there is some dilution of the fold planes with other molecules. Furthermore, the detailed stem arrangements presented here have been shown to give good agreement with infra-red results[32,33].

Some comment is necessary here on the extension of neutron scattering measurements into a molecular weight range where isotopic fractionation has been demonstrated previously by SANS[15]. The model derived has been shown to fit experimental data over the whole molecular weight range, with no change in the statistical arrangement of crystals stems other than an increase in the number of sheets. To this extent, any modification to molecular conformation arising from fractionation must only be a minor effect.

CONCLUSIONS AND GROWTH MECHANISMS

Intensity data for a wide range of q can now be assembled, for a range of molecular weights. What can be said at this stage about the crystallization mechanisms outlined in the Introduction? Firstly, the basic pattern of folding along {110} can now be taken as definitely established from the point of view of chain conformations. Secondly, a 'dilution' along the folded strips occurs by an alternation

of short folded sequences from different molecules. The mechanism of crystallization which leads to this alternation could in principle be of a Regime I type[19,20]. However, growth rate measurements at temperatures >70°C are not consistent with Regime I[34,35], and the theoretical predictions involve much longer adjacent sequences than the average figure of between 3 and 4 being proposed here. For the alternation to be due to independent attachment, as normally considered in Regime II, the attachment density would be very high indeed, approaching that recently proposed for Regime III crystallization (quench crystallization from the melt)[36].

The most promising explanation is probably in terms of growth on to a growth surface which has a degree of equilibrium-type roughness[22]. In this model, different parts of the molecule would be expected to attach independently. Favourable sites for attachment could be expected to be separated by several stems at 70°C. The model proposes that as temperature is increased the roughness increases until at ≈110°C it is sufficient for the faceted mode of growth to change to an unfaceted one. Measurements on crystals grown at 85°C are relevant here[9], for they suggest that the dilution is still present, though fractionation precludes more detailed study. Kinetic explanations (as alternatives to rough growth faces) would predict a small dilution at 85°C.

The results here are fully consistent with the superfolding proposed previously and the behaviour as a function of molecular weight can be given in more detail. The lengths of the sheets increase with molecular weight, but only to a small extent. The origin of this phenomenon is still unclear, but may well be kinetic.

ACKNOWLEDGEMENTS

Support for one of us (S.J.S.) from the SERC is acknowledged. The authors would like to thank Professor A. Keller for his comments and encouragement. The authors are also indebted to the staff of the Institut Laue Langevin (Grenoble) and AERE (Harwell) for assistance with neutron scattering measurements and to Mrs A. Halter for technical assistance in sample preparation and characterization.

REFERENCES

1 Keller, A. *Phil. Mag.* 1957, **2**, 1171
2 Keller, A. *Rep. Prog. Phys.* 1968, **31**, 623
3 Khoury, F. and Passaglia, E. 'Treatise on State Chemistry' (Ed N. B. Hannay) Plenum N.Y., 1976, p 335
4 Sadler, D. M. in "Structure of Crystalline Polymers" (Ed. I. Hall), Applied Science (London), 1984
5 Sadler, D. M. and Keller, A. *Colloid and Pol. Sci.* 1970, **239**, 641; and 1970, **242**, 1081
6 Patel, G. N. and Keller, A. *J. Polym. Sci. Phys. Ed.* 1975, **13**, 2259
7 Frank, F. C. and Tosi, M. *Proc. Roy. Soc.* 1961, **263A**, 323
8 Hoffman, J. D., Lauritzen, J. I., Passaglia, E., Ross, G. S., Frohlen, L. J. and Weeks, J. J. *Colloid and Pol. Sci.* 1969, **231**, 564
9 Sadler, D. M. and Keller, A. *Polymer* 1976, **17**, 37
10 Sadler, D. M. and Keller, A. *Macromolecules* 1978, **10**, 1128
11 Sadler, D. M. and Keller A. *Science* 1979, **203**, 263
12 Stamm, M., Fischer, E. W. and Dettenmaier, M. *Faraday Discussions* 1979, **68**, 263
13 Yoon, D. Y. and Flory, P. J. *Faraday Discussions* 1979, **68**, 288
14 Summerfield, G. C., King, J. S., and Ullman, R. *J. Appl. Cryst.* 1978, **11**, 548
15 Spells, S. J., Sadler, D. M. and Keller, A. *Polymer* 1980, **21**, 1121
16 Sadler, D. M. *Faraday Discussions* 1979, **68**, 419
17 Wignall, G. D., Mandelkern, L., Edwards, C. and Glotin, M. *J. Polym. Sci., Phys. Ed.* 1982, **20**, 245
18 Stamm, M. *J. Polym. Sci., Phys. Ed.* 1982, **20**, 235
19 DiMarzio, E. A. *J. Chem. Phys.* 1967, **47**, 3451
20 Sanchez, I. C. and DiMarzio, E. A. *J. Chem. Phys.* 1971, **55**, 893
21 Hoffman, J. D., Frohlen, L. J., Ross, G. S. and Lauritzen, J. I., *J. Res. Natl. Bur. Stand.* 1975, **79A**, 671
22 Sadler, D. M. *Polymer* 1983, **24**, 1401
23 Schmatz, W., Springer, T., Schelten, J. and Ibel, K. *J. Appl. Cryst.* 1974, **7**, 96
24 Haywood, B. C. G. and Worcester, D. L. *J. Phys. E.* 1973, **6**, 568
25 Jacrot, B. *Rep. Prog. Phys.* 1976, **39**, 911
26 Jacrot, B. and Zaccai, G. *Biopolymers* 1981, **20**, 2413
27 Guinier, A. *Ann. Phys., Paris* 1939, **12**, 161
28 Oster, G. and Riley, D. P. *Acta Cryst.* 1952, **5**, 272
29 Sadler, D. M. and Harris, R. *J. Polym. Sci., Phys. Ed.* 1982, **20**, 561
30 Bassett, D. C., Frank, F. C. and Keller, A. *Phil. Mag.* 1963, **8**, 1753
31 Sadler, D. M. *Faraday Discussions* 1979, **68**, 429
32 Spells, S. J., Keller, A. and Sadler, D. M. *Polymer* 1984, **25**, 749
33 Spells, S. J. *Polymer* 1984 (*Commun*), **24**, 162
34 Keller, A. and Pedemonte, E. *J. Crystal Growth* 1973, **18**, 111
35 Cooper, M. and St. J. Manley, R. *Macromolecules* 1975, **8**, 219
36 Hoffman, J. D. *Polymer* 1983, **24**, 3
37 Sadler, D. M. *J. Appl. Crystallogr.* 1983, **16**, 519